Modeling, analysis and characterization of ionic electroactive polymers based tri-layer micro-actuators

Sofiane Ghenna, Lauréline Seurre, Caroline Soyer, Héléne Arena, Sébastien Grondel, Eric Cattan

Modeling, analysis and characterization of ionic electroactive polymers based tri-layer micro-actuators

S. Ghenna, L. Seurre, C. Soyer, H. Arena, S. Grondel, and E. Cattan

Univ. Polytechnique Hauts-de-France, CNRS, Univ. Lille, Yncrea, Centrale Lille, UMR 8520 -IEMN, DOAE, 59313 Valenciennes, France

ABSTRACT

In this paper, the electrical response of ionic electro-active polymer (IEAP) based tri-layer micro-actuator allowing to consider some phenomena which occur in the micro-actuator behavior is presented. A detailed study on the measured currents during charging and discharging process is analyzed. Electrical charges, time constants, capacitance and resistance of the simplified equivalent electrical circuit are investigated. The results have shown that, the micro-actuator exhibits a linear behavior for applied voltage lower than 1 V. Beyond that, non-linearities appear and are related to the discharging process, especially the corresponding electrical resistance which increases in a non-linear way. At this stage, accumulated electrical charges which depend on the previously applied voltage are not totally restored during the discharging process. The results of this study are illustrated with experimental and theoretical results.

Keywords: Modeling, characterization, identification, ionic electro-active polymers, micro-actuators

1. INTRODUCTION

IEAP based actuators have specific characteristics that allow them to be now used for various applications, whether in applications requiring actuation and/or sensor functions. The main advantage of these actuators compared to piezoelectric or dielectric actuators relies on ability to provide large deformations for a low actuation voltage ($\sim 2\,V$), representing promising materials for MEMS. However, IEAP actuators velocity is far behind of piezoelectric actuators due to the migration of ions which can be slow. Moreover, their mechanical force is still weak due to their very low electromechanical coupling (under 1%),[1,2] leading to low efficiency. Nevertheless, their low cost, light weight, noise-free operation,[3] their long life cycle[4] without degradation make IEAP based actuators a promising technology for specific integrations.[5] In the literature, there is a large number of publications covering the different types of linear[6] or flexural micro-actuators,[7] operating in solution[8] or in ambient air conditions.[9] Due to these advantages, they are implemented in a wide range of applications.[2,3,5,7,8]

The operating principle of IEAP micro-actuators is based on the mobility of cations in the polymer network when an electrical voltage is applied. For conducting polymer actuator, it was reported that a bending motion is generated according to the simultaneous oxidation-reduction process.[2] This, leads respectively to an expansion on one electrode of the actuator and a contraction on its other side. Therefore, both electrodes push the trilayer to the same side and add their contribution to the movement. In fact, the electrical, mechanical, and chemical responses of these micro-actuators are interdependent,[10] and influence the responses to a stimulus. Hence, development of IEAP based micro-actuator requires improved theoretical and empirical understanding of their behavior. Different approaches on the modeling of IEAP micro-actuators have been proposed,[10–12] most of them consider the electronically part as resistance and use capacitance electrical circuit to represent the charging process. The electromechanical coupling is based on the relationship between the strain and the volumetric charge density,[1] while the mechanical part introduces Euler-Bernoulli dynamic beam equations.[11] A number of experimental validations have been conducted highlighting the predictive properties of the models. However these works didn't analyze the charging and discharging process under DC voltage especially with relatively long time period. Moreover the presence of a possible non-linearity such as memory effect or hysteresis behavior has not been analyzed. In,[13] the authors proposed a simple model of polymeric relaxation (operating in aqueous

Further author information: (Send correspondence to S.G)
S.G.: E-mail: sofiane.ghenna@uphf.fr, Telephone: +33 3 27 51 14 45

solution) based on description of the form of chronoamperograms. Moreover, the micro-actuator has been treated from an electrochemical point of view.
In this paper, a flexural IEAP trilayer micro-actuator operating in air is investigated. The study focuses on the electrical response over a relatively long period, allowing in one hand to consider some non-linearity which occur on the micro-actuator, and in the other hand to identify equivalent electrical parameters even in natural discharging process. Hence, this paper is organized as follow: in the first part, a brief electrical model is presented. In the second part, analysis and characterization of IEAP based micro-actuator is introduced, including input current measurement in response to an applied voltage, electrical charges accumulated during charging and discharging process, resistance and capacitance behavior in function of applied voltage. Finally, identification methodology for the IEAP micro-actuator is addressed.

2. MODELING OF IEAP BASED TRILAYER MICRO-ACTUATORS

2.1 Electrochemical model

The central layer of IEAP based trilayer micro-actuators is considered as an ion reservoir providing the system with ionic conductivity and mechanical properties.[14] It it formed with a semi-interpenetrated polymer network (IPN) composed of two polymers; poly(ethylene oxide) PEO and linear nitrile butadiene rubber NBR network as depicted in Fig. 1b. Electrodes are made of a conducting polymer poly(3,4-ethylenedioxythiophene): poly(styrene sulfonate) called PEDOT:PSS/PEO as reported in.[14,15] The obtained trilayer is filled with ionic liquid 1-ethyl-3-methylimidazolium (EMIm+), bis-trifluoromethyl sulfonyl-imide (TFSI-).[16,17] During the oxidation process, the cations leave the electrode with positive potential to balance charges, leading to the expansion of the cathode. At the other electrode with negative potential, cations are injected by a diffusion process,[11,18] leading to the compression of the anode. These opposite and concomitant movements lead consequently to bending deformation of micro-actuator. The bending direction is occurring toward the anode.[16] For a bilayer conducting polymer in solution, this process has been modeled by circuit model where a resistance and capacitance circuit are associated with an impedance of ions diffusing into or out of the polymer.[19,20] Similarly, and for trilayer actuator, 2D diffusion transmission line across the thickness and the length of a trilayer actuator is developed in.[11]
In this paper, the modeling of the micro-actuator is considered along 1D. Hence, the diffusion through the electrode thickness is neglected. The oxidation process can be modeled by electrode resistance R_e and electric layer capacitance C_L circuit for each electrode (see Fig. 1.a). The electrolyte resistance to the transfer of ions in the central layer is modeled by a resistance R_{ion}, while the short circuit resistance between electrodes is modeled by R_s. R_g and R_w represent respectively gold contact and copper wire resistance.

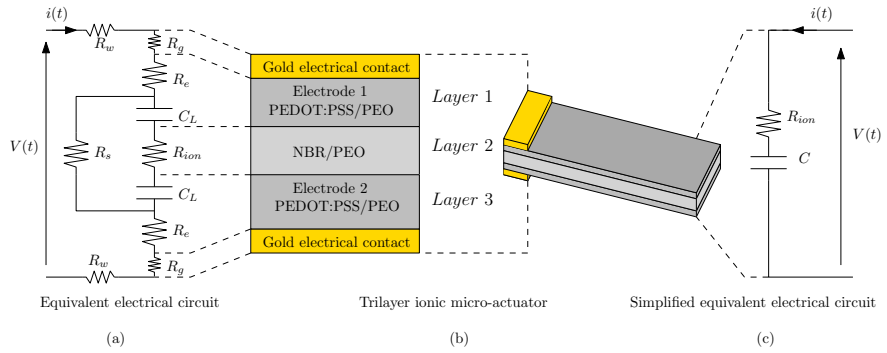

Figure 1: IEAP trilayer based micro-actuator configuration with its 1D equivalent electrical circuit.

2.2 Simplified electrochemical model

In order to predict the electrical dynamic behavior under applied voltage and evaluate critical parameters affecting actuation performances, the simplified model is adopted. In this work, the resistivity of the electrode has been measured (7.142 µΩ m) allowing to neglect the transmission line R_e. The gold R_g and copper wire R_w resistances are supposed very low, while the resistance R_s parallel to R_{ion} is supposed very high allowing them to be neglected

with respect to R_{ion} (these assumptions will be validated in the later parts of this paper). Moreover, both serial capacitances C_L are supposed identical and presented by an equivalent double layer capacitance C as presented in Fig. 1.c. The voltage across the $R_{ion}C$ circuit, which is time-dependent, can be expressed as:

$$V(t) = R_{ion} i(t) + \frac{1}{C} \int i(t)\,\mathrm{d}t \tag{1}$$

where

$$\int i(t)\,\mathrm{d}t = Q(t) \tag{2}$$

$Q(t)$ is the accumulated electrical charges, by substituting Eq (2) in Eq (1), Eq (1) becomes

$$CV(t) = \tau \frac{dQ(t)}{dt} + Q(t) \tag{3}$$

where $\tau = R_{ion}C$ is the time constant. In steady state, $\frac{dQ(t)}{dt} = 0$ which gives:

$$CV(t) = Q(t) \tag{4}$$

3. ANALYSIS AND CHARACTERIZATION OF IEAP BASED MICRO-ACTUATORS

In this part, IEAP based trilayer micro-actuator was micro-fabricated according to the method described in.[7] Then, the behavior of micro-actuator beam with dimensions of $6.67 \times 1.37 \times 0.035$ mm^3 (given in Fig. 2) was examined from an electrical point of view. For this purpose, experiments were carried out under potentiostat

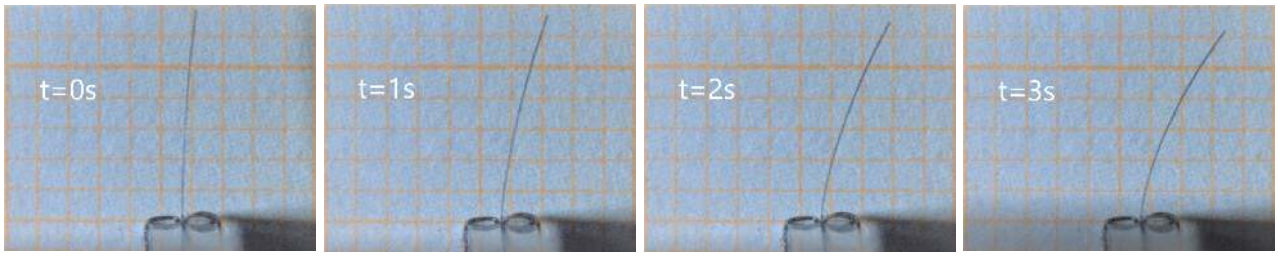

(a) (b) (c) (d)

Figure 2: Response of the studied IEAP micro-actuator subjected to a square voltage amplitude of 1.5 V and frequency of 0.1 Hz, pictures (from left to right) taken at different times.

600^{TM} of Gamry instruments (in chronoamperometry mode allowing to measure currents of the order of micro-Ampere). In order to analyze the charging process, a positive square voltage was applied to a new micro-actuator* and a zeroing of the voltage was imposed on the discharging process. It has been verified that setting the voltage to 0 V in fact corresponds to short-circuiting of the actuator. The micro-actuator was excited with different voltage levels and according to the falling edge from 1.75 to 0.5 V with a step of 0.25V as shown in Fig. 3.

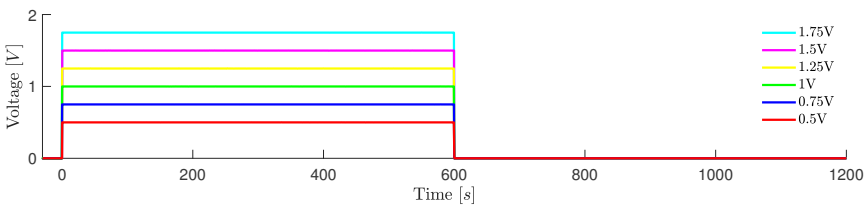

Figure 3: Applied voltage to the trilayer micro-actuator

*The micro-actuator has never been used, avoiding the influence of actuator fatigue and ageing effect on its behavior.

In the second step, the same experience was repeated in the same micro-actuator, but in this case, the micro-actuator was excited according to the rising edge of the voltage from 0.5, to 1.75V with a step of 0.25V in order to verify the presence of any non-linearity. All measurements were carried out over a period of 1200 s (600 s for each charging and discharging process) to ensure that the response time is sufficient to charge or discharge the actuator from an electrical point of view. Furthermore, to ensure that after discharging process, the micro-actuator returns near its initial position from a mechanical point of view.

3.1 Measurement of micro-actuator input current in response to an applied voltage

The raw measured current at room temperature is presented in Fig. 4 at the charging (left column) and discharging (right column) process, according to the falling (top row) and rising (bottom row) edge of the applied voltage. The duration of both processes is sufficiently long, which allows the current to fall back practically to zero. It should be noted that, the measured current presents a certain offset of the current $I_0 = 9.25 \times 10^{-5}$ A due to the measuring device. Otherwise, from the waveform of the current, it's obvious that, the micro-actuator exhibits a non-faradaic (capacitive) process.[21] This capacitive current is positive during the charging process, reaches a maximum value and comes back to zero and inversely for the discharging process.
As can be seen, in the charging process, the current peak increases with increasing voltage, however this is not the case for the discharging process with regard to voltages above 1 V. This nonlinear behavior will be examined in detail in the following parts.

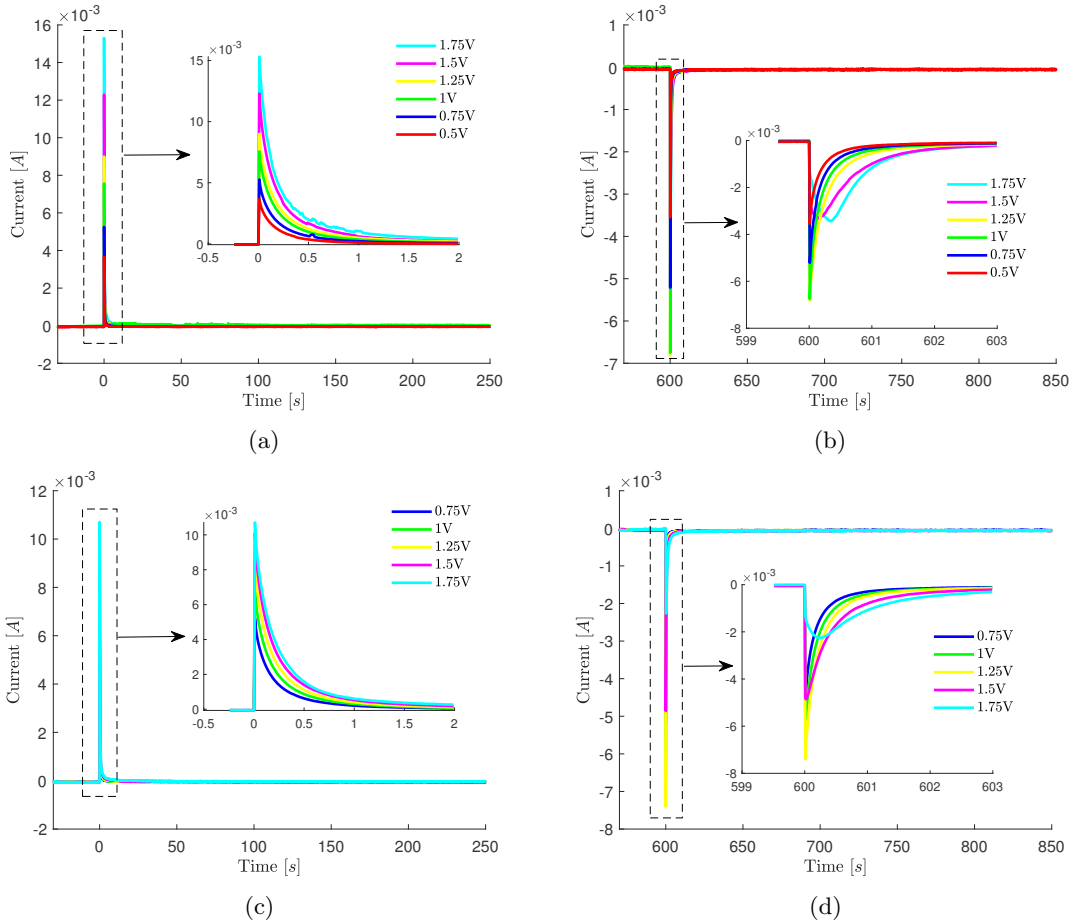

Figure 4: Measured currents with zoom on the transient regime for different voltage levels, according to charging ((a) and (c)) and discharging [(b) and (d)] process, with respect to voltage falling edge [((a) and (b)]and rising edge [(c) and (d)].

3.1.1 Analysis of experimental current curves

The objective of this part is to create the current curves from mathematical functions, therefore to identify the parameters of the simplified model. Since the adopted model is an $R_{ion}C$ circuit and since current curves are exponential responses (capacitive current), then the identification will be made with exponential mathematical functions using MATLAB® *fitnlm* function. The fitted results showed that, the best curve fitting is obtained with summation of three exponential functions associated with an offset current ($\sum_{i=1}^{n=3} A_i e^{\frac{-t}{\tau_i}} + I_0$) as illustrated in Fig. 5 as an example for an applied voltage of 1 V. Indeed, this is justified by the simplification and hypothesis introduced in the $R_{ion}C$ circuit. In fact, the fitted curves which correspond to the introduced hypotheses are represented by n = 1. Hence, from n = 1, the time constant $\tau = R_{ion}C$ for all measurements is presented in

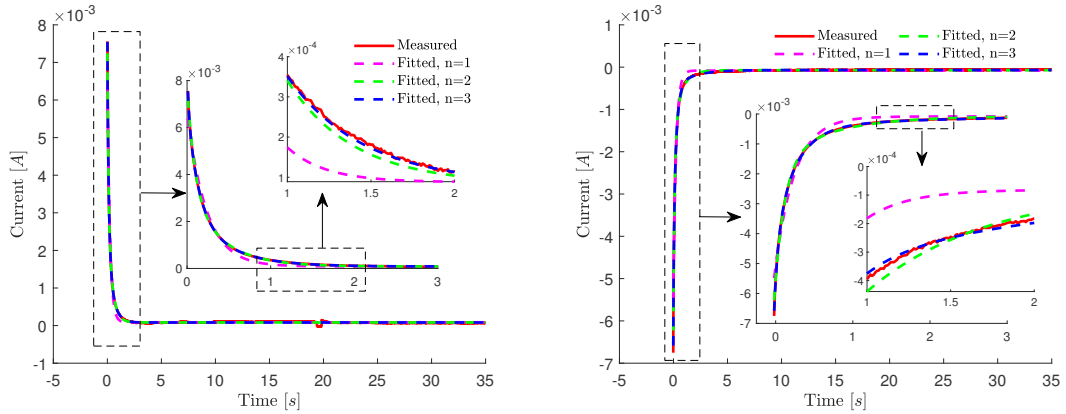

(a) (b)

Figure 5: Measured current at 1 V with zoom on the transient regime during the charging (a) and discharging process (b), and fitted with $\sum_{i=1}^{n} A_i e^{\frac{-t}{\tau_i}} + I_0$, where n = {1, 2, 3}.

Fig. 6. Examination of fitted current curves with n = 1 shows practically a similar level of time constant between both charging processes. In addition, the same level was practically obtained for both discharging processes lower than 1 V. This means that, there is not a notable variation on the $R_{ion}C$ product for voltage levels lower than 1 V, whether depending on the rising or falling edge, whether depending on the charging or discharging process. In the other case (> 1 V), it seems that, the discharging process is done with more slowly behavior. Additionally,

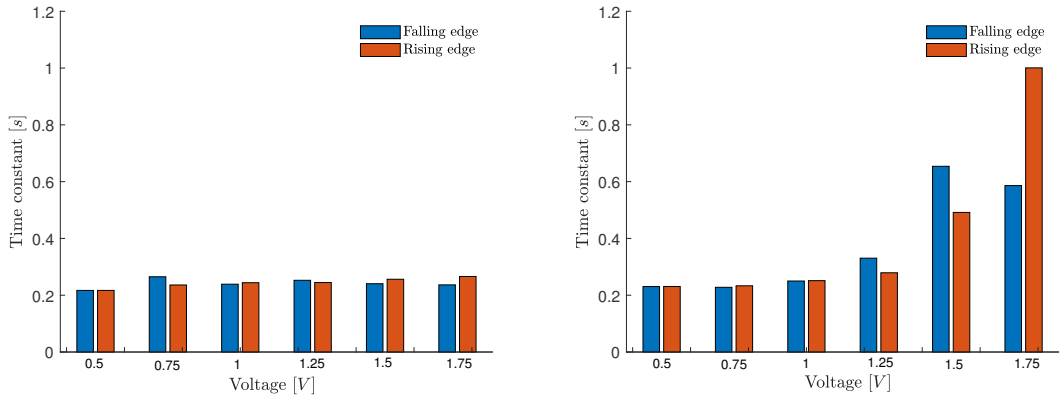

(a) (b)

Figure 6: Identified time constant τ_1 for diffirent applied voltages according to falling and rising edge with respect to charging (a) and discharging (b) process.

there is a notable difference on the time constants according to falling and rising edge. This non-linearity is discussed hereafter.
For the rest of this paper, the behavior of the micro-actuator is examined with n = 3 for a more precise results. A comparison between them (n = {1, 3}) is reported in the last part.

3.2 Electrical charges accumulated at charging and discharging process

The phenomenon of accumulated charges on IEAP micro-actuator is one of critical parameters allowing understanding its operation principle and behavior. Since micro-actuator strain is related to the volumetric charge density,[1] therefore it is important to grasp its charge amounts and to understand why the micro-actuator does not return exactly to its initial position during the discharging process.

3.2.1 Measurement method of accumulated electric charges

The accumulated charges during the charging (positive charges) and discharging (negative charges) process are determined independently by applying Eq (2). For this purpose, MATLAB® *cumtrapz* function (cumulative trapezoidal numerical integration) is applied to the measured current presented in Fig. 4 and without taking into account the offset current $I_0 = 9.25 \times 10^{-5}$ A, while the fitted accumulated charges are calculated by integration of the corresponding identified exponential function as presented in Fig. 7. As expected, successive increasing / decreasing DC electrical voltages with the same polarity promote an increase / decrease of accumulated charges. However, this is not always true for the discharging process, especially above 1 V.

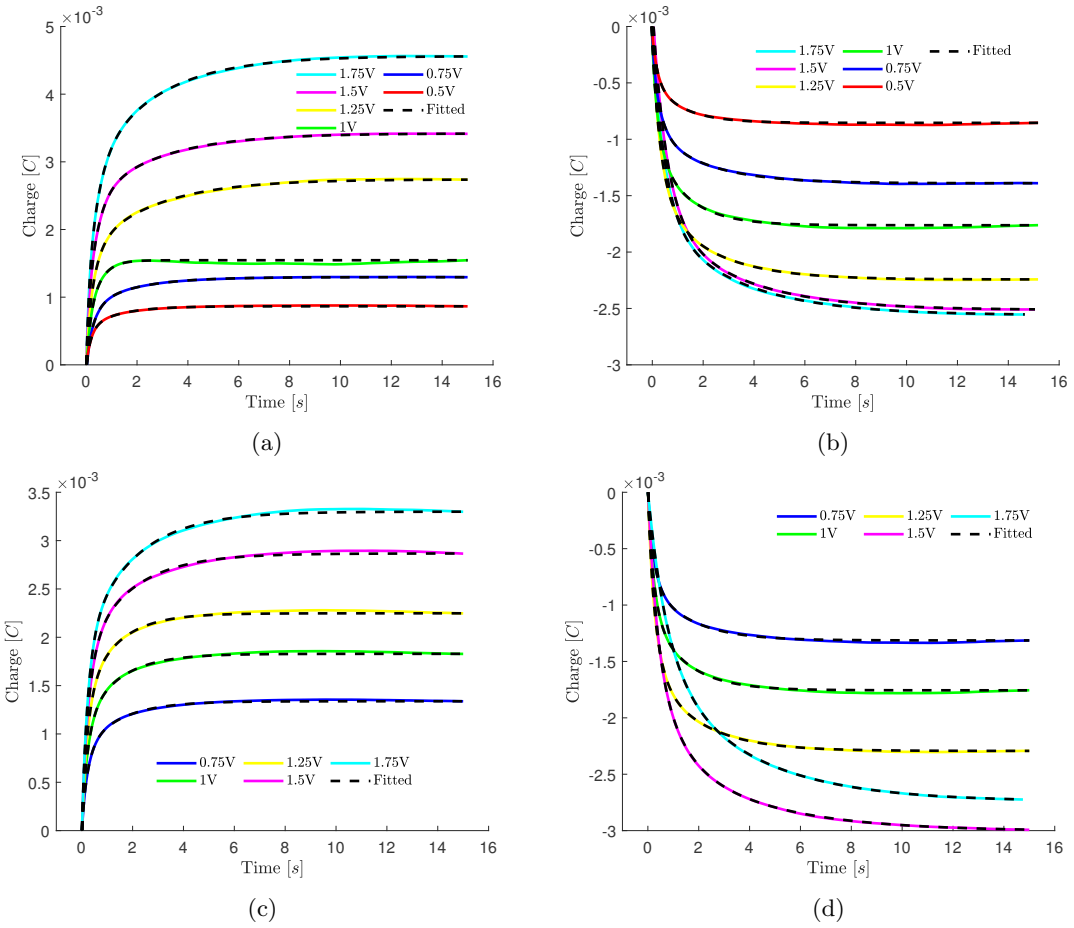

Figure 7: Accumulated electrical charges for different voltage levels, according to charging [(a) and (c)] and discharge [(b) and (d)] process, with respect to voltage falling edge [(a) and (b)] and rising edge [(c) and (d)].

3.2.2 Cumulative, restored and remanent electric charges

The accumulated electrical charges are determined in steady state (when the equilibrium of the accumulated charges is reached), and are summarized in Fig. 8. In order to facilitate understanding and curves comparison, a nearest neighbor method is adopted for curves representation. For this, cumulative (positive charges), restored (negative charges) and remanent charges (difference between both processes) as a function of the applied electrical voltage are presented in the top row (left: falling edge, right: rising edge), while the bottom row represents a comparison between accumulated charges (left) and restored charges (right), according to falling and rising edge of the applied voltage. This study allowed showing the dependency between the charging and discharging process. This dependency shown in Fig. 8a, can be interpreted as a memory effect.[22] Indeed, since positive square voltages are applied to the micro-actuator with time period sufficiently long, the micro-actuator does not fully discharge the charges accumulated previously during the discharging process (green curves). Moreover, the results show that, according to the falling edge, non-linearities appear beyond 1 V as confirmed previously in Fig. 6. This is manifested by the presence of the remaining charges. It seems that, during the oxidation process, when cations leave the cathode, they do not fully return to their natural position during discharging process which can justify the non-auto-resetting of the micro-actuator to its initial state (zero position) after discharging process. However, with rising edges of applied voltage less than 1.5 V (Fig. 8b), the charging and discharging process are similar. The comparison between both charging processes (according to falling and rising edge) shows that, the two curves are diverging (> 1 V) and presents a memory effect as well (Fig. 8c). However, the two

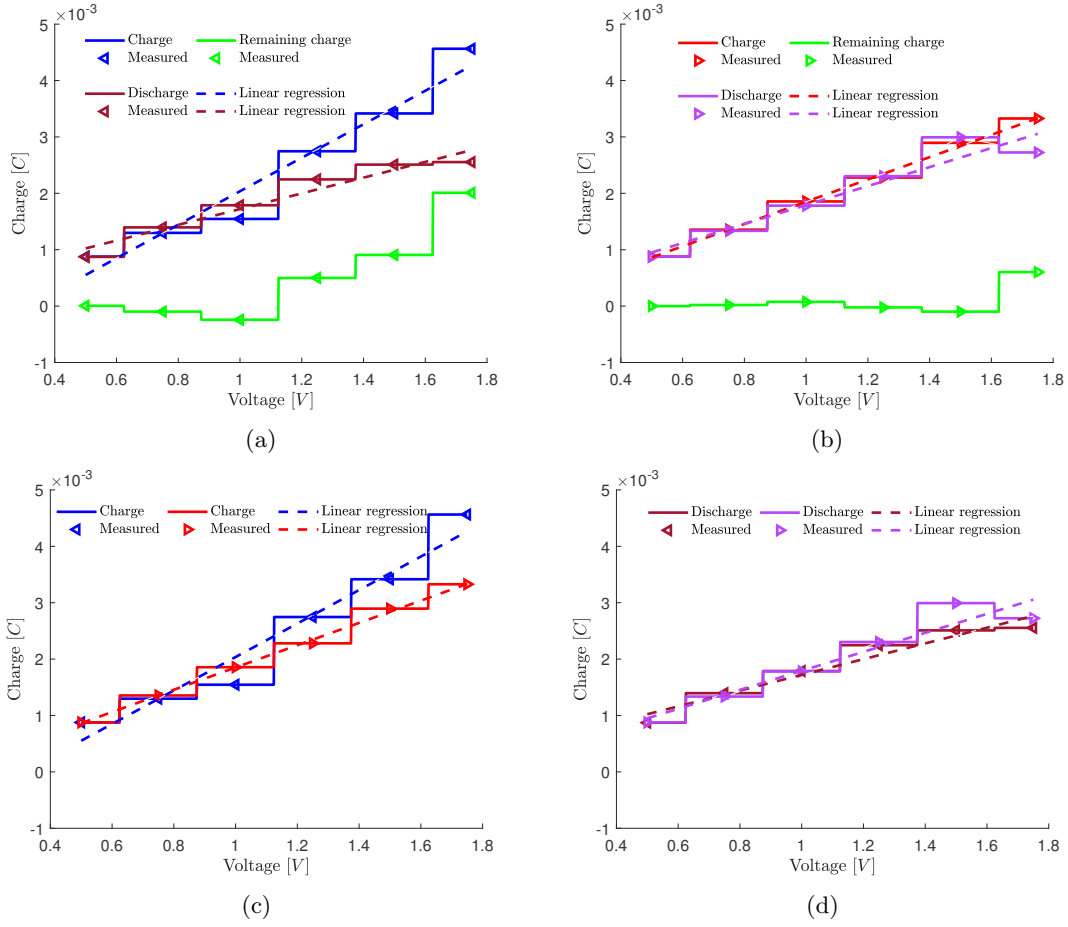

Figure 8: Electrical charges as a function of applied voltage, according to voltage falling edge (a) and rising edge (b), (c) and (d) comparison between charging and discharging process respectively with respect to both voltage falling edge and rising edge. Arrows indicate the applied edge direction.

discharging processes are practically not affected by this effect (Fig. 8d).

3.3 Simplified model parameter identification

In this work, in order to identify parameter of the simplified model described in Fig. 1.c, the current peaks will be used for the determination of the equivalent electrical resistance R_{ion} by applying Ohm's law, while the accumulated electrical charges will be used to determine the capacitance C according to Eq (4) and therefore the time constant τ.

3.3.1 Equivalent electrical resistance

When voltage $V = V_c$ is applied (t_c=0 s) or short-circuited $V = V_d = 0$ (t_d=600 s) corresponding to current peak charge i_c or discharge i_d (see Fig. 4), the micro-actuator behaves like a pure resistance. Hence, the equivalent resistance R^{k}_{ion} is determined according to Eq (5) and presented in Fig. 9.

$$R^{\mathrm{k}}_{ion} = \frac{V_c}{i_k} \quad \text{where k} = \{\mathrm{c,d}\} \tag{5}$$

If time constants at discharging process present a non-linearity above 1 V (Fig. 6b), and if the restored charges are considered linear (Fig. 8d), then the responsible for this non-linearity in the discharging process is the resistance R^{d}_{ion} as identified in Fig. 9b. A high resistance that opposes to the passage of cations results in a

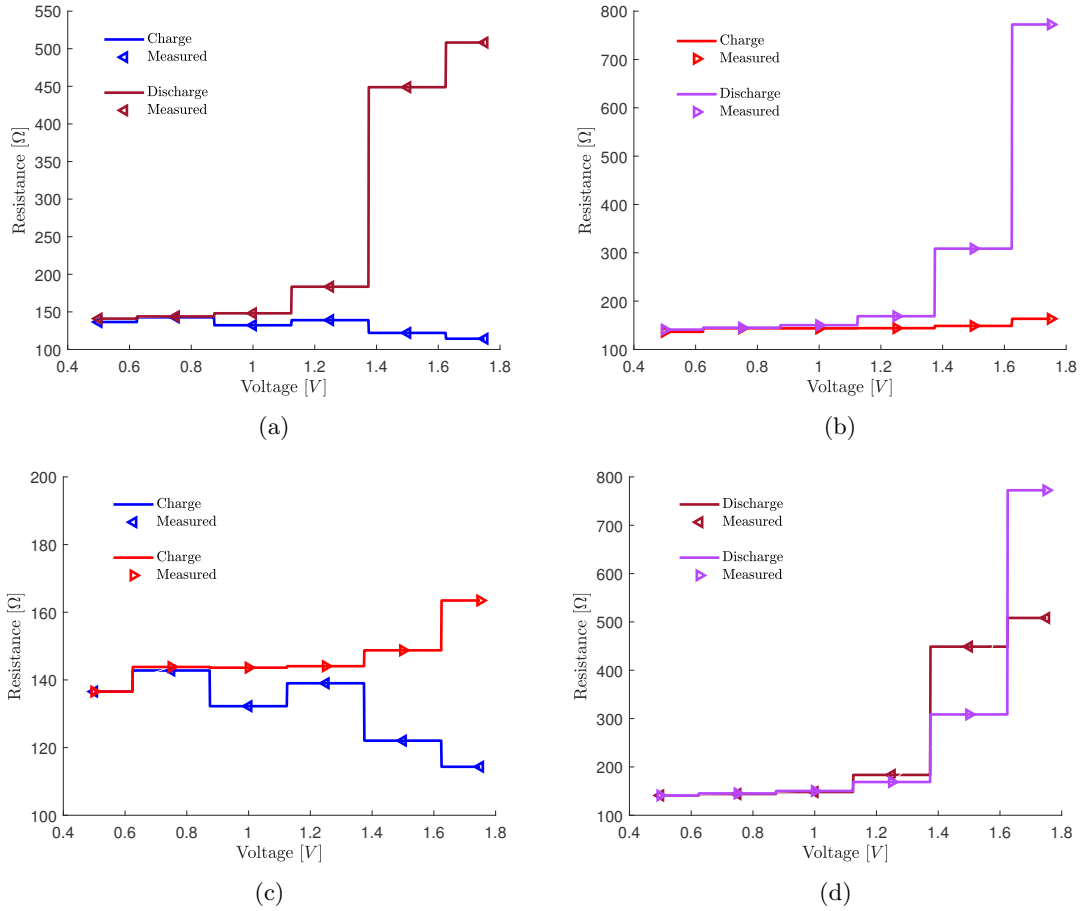

Figure 9: Equivalent electrical resistance as a function of applied voltage, according to voltage falling edge (a) and rising edge (b), (c) and (d) comparison between resistance measured at charging and discharging process respectively with regard to both voltage falling edge and rising edge. Arrows indicate the applied edge direction.

decreasing rate of cation transfer. Therefore, this is manifested by the presence of the remaining charges as discussed in subsection 3.2.2. As for the charging resistance R^{c}_{ion} (Fig. 9c), it seems that, with relatively high voltage (depending on the rising or falling edge) a difference of 70% can be obtained between them. Indeed, the cations do not have the same transfer speed in both directions (falling and rising edge) which could be linked to the memory effect. Furthermore, more the voltage is decreased, more a linear behavior in terms of resistance variation is obtained (Fig. 9a) and consequently leading to an uniform cation transfer rate.
From another angle, when the time constants are increasing (discharging process $> 1\,\mathrm{V}$), consequently cations speeds are decreasing. Then, more time is required for cations to return to their initial positions. Mechanically, more time is required for the micro-actuator to return to its initial position in term of deformation.
Because of non-linear R^{d}_{ion} behavior, only R^{c}_{ion} is summarized in Fig. 10a. The results show that, according to the falling edge, the average of measured electrical cation resistances $(131.1613 \pm 10.8943)\ \Omega$ is lower than that measured according to the rising edge $(146.7143 \pm 9.0911)\ \Omega$. In terms of decreasing of resistance, the same behavior is obtained according to the discharging process (Fig. 9d).
For the resistance R_s which was neglected in this study, and by substitution the measured offset current ($I_0 = 9.25 \times 10^{-5}\,\mathrm{A}$) from current measurements (Fig. 4), the leakage current has not been observed, i.e., no current has been crossing the trilayer, which means the resistance R_s is very high. Thus, the previously introduced hypotheses are validated.

3.3.2 Equivalent electrical capacitance

In Fig. 10b, the average of capacitance ($Q(t)/V(t)$ from Fig. 8) according to falling and rising edge with respect to charging and discharging process over different experimental measurements is presented to highlight capacitance behavior and identification. The standard deviation is calculated as the square root of variance by determining each capacitance deviation relative to the average. Identified capacitance on all measurements are really close. Moreover, even if standard deviations can intersect, according to the charging process, the results show that the capacitance of the falling edge is slightly higher than that measured according to the rising edge. This point could justify the high value of accumulated charge for the first measurement (1.75 V) carried out as shown in Fig. 8a.

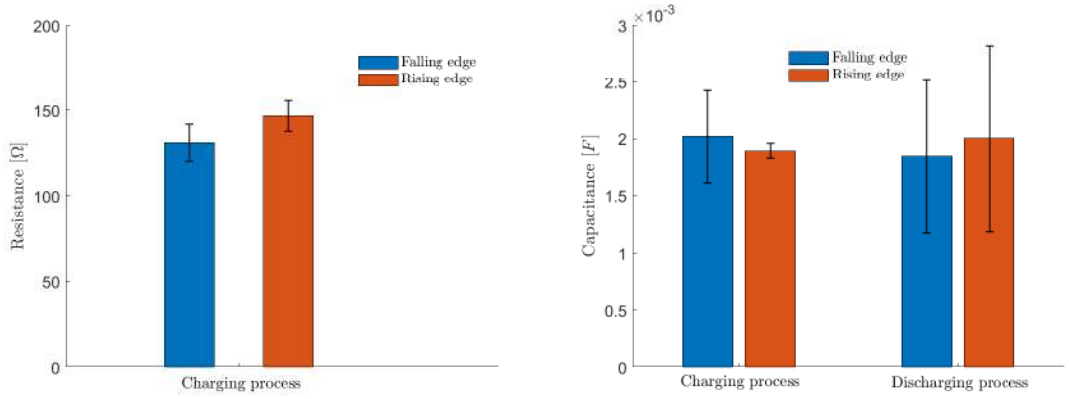

(a) (b)

Figure 10: Average with standar deviation of different experimental measurements, (a) equivalent electrical resistance and (b) capacitance.

3.3.3 Time constant

For comparison purposes according to the charging process, identified time constants with fitted current curves corresponding to n=1 (Fig. 6a) are compared with the measured time constant ($\tau_c = R^{c}_{ion}C^{c}$ from Fig. 10) and summarized in Fig. 11.
Even if the time constant determined by the fitted curves have been fitted with n = 1, nevertheless they agree

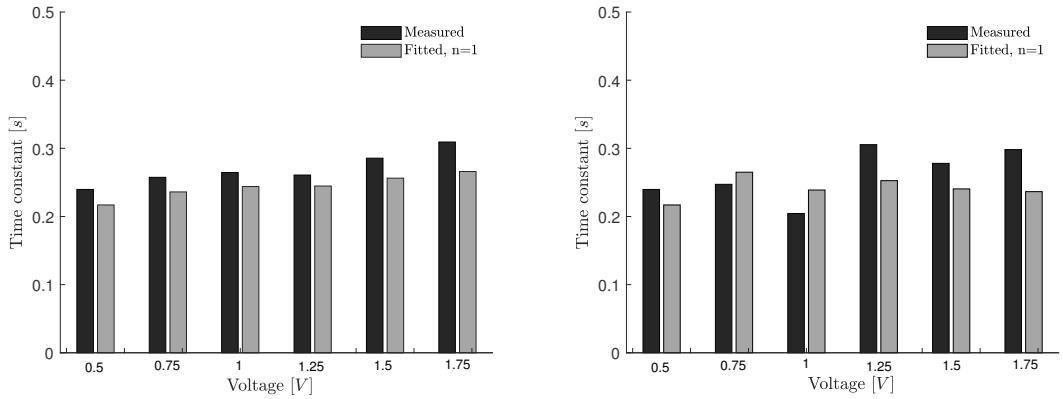

(a) (b)

Figure 11: Comparison between identified time constants with fitted current curves (n=1) and measured with ($\tau_c = R^c_{ion}C^c$) according to charging process, for diffirent applied voltages, (a) falling edge and (b) rising edge.

well with the practical identification with an average precision of 92% for the falling edge and 90% for the rising edge. Hence the validation of the proposed approach is approved.

4. CONCLUSION

In this paper, IEAP based trilayer micro-actuator is investigated from an electrical point of view allowing to consider non-linearity which occurs in the micro-actuator. A simplified electrical model is presented, then a detailed study on the capacitive current during charging and discharging process is analyzed according to falling and rising edge of applied voltage. The micro-actuator exhibits a linear behavior for applied voltage lower than 1 V. Non-linearities that appear above 1 V are related to the discharging process especially the resistance which increases in a non-linear way. The discharging resistance influences massively on the transfer or mobility of cations and is manifested by the presence of the remaining charges. This, can justify the non auto-resetting of the micro-actuator to its initial state after discharging process from a mechanical point of view. Moreover, the dependency between the charging and discharging process can be interpreted as a memory effect where electrical charges depend on the previously applied voltage. Finally, model identification parameters are proposed and showing a good agreement between the two methods.
Future work should focus on both mechanical and electrical aspects. In addition, identification methodology for IEAP based micro-actuators with different geometric parameters and demonstrating the relationship between their geometric and dynamic parameters would be interesting.

ACKNOWLEDGMENTS

This work was supported by H2020 project TWINNIMS (Grant agreement 857263), by the French Government through the National Research Agency (ANR) and project MicroTIP, ROBOCOP, PIA EQUIPEX LEAF (ANR-11-EQPX-0025) and by the French RENATECH network.

REFERENCES

[1] Madden, J. D. W., Vandesteeg, N. A., Anquetil, P. A., Madden, P. G. A., Takshi, A., Pytel, R. Z., Lafontaine, S. R., Wieringa, P. A., and Hunter, I. W., "Artificial muscle technology: physical principles and naval prospects," *IEEE Journal of Oceanic Engineering* **29**(3), 706–728 (2004).

[2] Kim, K. J. and Tadokoro, S., "Electroactive polymers for robotic applications," *Artificial Muscles and Sensors* **23**, 291 (2007).

[3] Must, I., Kaasik, F., Põldsalu, I., Mihkels, L., Johanson, U., Punning, A., and Aabloo, A., "Pulse-width-modulated charging of ionic and capacitive actuators," in [*2014 IEEE/ASME International Conference on Advanced Intelligent Mechatronics*], 1446–1451 (2014).

[4] Vidal, F., Plesse, C., Teyssié, D., and Chevrot, C., "Long-life air working conducting semi-ipn/ionic liquid based actuator," *Synthetic Metals* **142**(1), 287 – 291 (2004).

[5] Smela, E., "Conjugated polymer actuators for biomedical applications," *Advanced Materials* **15**(6), 481–494 (2003).

[6] Ghaffari, M., Kinsman, W., Zhou, Y., Murali, S., Burlingame, Q., Lin, M., Ruoff, R. S., and Zhang, Q. M., "Retracted: Aligned nano-porous microwave exfoliated graphite oxide ionic actuators with high strain and elastic energy density," *Advanced Materials* **25**(43), 6277–6283 (2013).

[7] Seurre, L., Rohtlaid, K., Nguyen, G. T. M., Soyer, C., Ghenna, S., Grondel, S., Vidal, F., Cagneau, B., Plesse, C., and Cattan, E., "Demonstrating full integration process for electroactive polymer microtransducers to realize soft microchips," in [*2020 IEEE 33rd International Conference on Micro Electro Mechanical Systems (MEMS)*], 917–920 (2020).

[8] Otero, T. F., "Towards artificial proprioception from artificial muscles constituted by self-sensing multi-step electrochemical macromolecular motors," *Electrochimica Acta* **368**, 137576 (2021).

[9] Must, I., Vunder, V., Kaasik, F., Põldsalu, I., Johanson, U., Punning, A., and Aabloo, A., "Ionic liquid-based actuators working in air: The effect of ambient humidity," *Sensors and Actuators B: Chemical* **202**, 114 – 122 (2014).

[10] Bentefrit, M., Grondel, S., Soyer, C., Fannir, A., Cattan, E., Madden, J. D., Nguyen, T. M. G., Plesse, C., and Vidal, F., "Linear finite-difference bond graph model of an ionic polymer actuator," *Smart Materials and Structures* **26**, 095055 (aug 2017).

[11] Nguyen, N. T., Dobashi, Y., Soyer, C., Plesse, C., Nguyen, G. T. M., Vidal, F., Cattan, E., Grondel, S., and Madden, J. D. W., "Nonlinear dynamic modeling of ultrathin conducting polymer actuators including inertial effects," *Smart Materials and Structures* **27**, 115032 (oct 2018).

[12] John, S., Alici, G., and Cook, C., "Frequency response of polypyrrole trilayer actuator displacement," in [*Electroactive Polymer Actuators and Devices (EAPAD) 2008*], Bar-Cohen, Y., ed., **6927**, 565 – 572, International Society for Optics and Photonics, SPIE (2008).

[13] Otero, T. F., Grande, H.-J., and Rodríguez, J., "Reinterpretation of polypyrrole electrochemistry after consideration of conformational relaxation processes," *The Journal of Physical Chemistry B* **101**(19), 3688–3697 (1997).

[14] Plesse, C., Vidal, F., Randriamahazaka, H., Teyssié, D., and Chevrot, C., "Synthesis and characterization of conducting interpenetrating polymer networks for new actuators," *Polymer* **46**(18), 7771 – 7778 (2005). Stimuli Responsive Polymers.

[15] Khaldi, A., Plesse, C., Soyer, C., Cattan, E., Vidal, F., Legrand, C., and Teyssié, D., "Conducting interpenetrating polymer network sized to fabricate microactuators," *Applied Physics Letters* **98**(16), 164101 (2011).

[16] Rohtlaid, K., Seurre, L., Nguyen, G. T. M., Curley, G., Soyer, C., Grondel, S., Vidal, F., Plesse, C., and Cattan, E., "PEDOT:PSS-based micromuscles and microsensors fully integrated in flexible chips," *Smart Materials and Structures* **29**, 09LT01 (jul 2020).

[17] Nguyen, T. N., Rohtlaid, K., Plesse, C., Nguyen, G. T., Soyer, C., Grondel, S., Cattan, E., Madden, J. D., and Vidal, F., "Ultrathin electrochemically driven conducting polymer actuators: fabrication and electrochemomechanical characterization," *Electrochimica Acta* **265**, 670 – 680 (2018).

[18] Proctor, C. M., Rivnay, J., and Malliaras, G. G., "Understanding volumetric capacitance in conducting polymers," *Journal of Polymer Science Part B: Polymer Physics* **54**(15), 1433–1436 (2016).

[19] Madden, P. G. A., Madden, J. D. W., Anquetil, P. A., Vandesteeg, N. A., and Hunter, I. W., "The relation of conducting polymer actuator material properties to performance," *IEEE Journal of Oceanic Engineering* **29**(3), 696–705 (2004).

[20] Okuzaki, H., Takagi, S., Hishiki, F., and Tanigawa, R., "Ionic liquid/polyurethane/pedot:pss composites for electro-active polymer actuators," *Sensors and Actuators B: Chemical* **194**, 59 – 63 (2014).

[21] Biesheuvel, P. M., Porada, S., and Dykstra, J. E., "The difference between faradaic and non-faradaic electrode processes," (2021).

[22] Vorotyntsev, M. A., Skompska, M., Pousson, E., Goux, J., and Moise, C., "Memory effects in functionalized conducting polymer films: titanocene derivatized polypyrrole in contact with thf solutions," *Journal of Electroanalytical Chemistry* **552**, 307 – 317 (2003). Special volume dedicated to Professor Boris B. Damaskin on the occasion of his 70th birthday.